A new Lagrange multiplier approach for gradient flows

Qing Cheng[a], Chun Liu[a,1], Jie Shen[b,*,2]

[a] *Department of Applied Mathematics, Illinois Institute of Technology, Chicago, IL 60616, USA*
[b] *Department of Mathematics, Purdue University, West Lafayette, IN 47907, USA*

Abstract

We propose a new Lagrange multiplier approach to design unconditional energy stable schemes for gradient flows. The new approach leads to unconditionally energy stable schemes that are as accurate and efficient as the recently proposed SAV approach (Shen, Xu, and Yang 2018), but enjoys two additional advantages: (i) schemes based on the new approach dissipate the original energy, as opposed to a modified energy in the recently proposed SAV approach (Shen, Xu, and Yang 2018);and (ii) they do not require the nonlinear part of the free energy to be bounded from below as is required in the SAV approach. The price we pay for these advantages is that a nonlinear algebraic equation has to be solved to determine the Lagrange multiplier. We present ample numerical results to validate the new approach, and, as a particular example of challenging applications, we consider a block copolymer (BCP)/coupled Cahn–Hilliard model, and carry out new and nontrivial simulations which are consistent with experiment results.
© 2020 Elsevier B.V. All rights reserved.

1. Introduction

Gradient flows play an important role in science and engineering as a large class of mathematical models which can be described by PDEs in the form of gradient flow, some particularly interesting examples include: crystal growth [1–3], solidification [4–6], tumor growth [7,8], thin film [9,10], liquid-vapor phase transformations [11,12], fracture mechanics [13,14].

How to design efficient and energy stable numerical schemes for gradient flows has attracted much attention in recent years, we refer to [15] for a up-to-date extensive review on this subject. In particular, the recent proposed SAV approach [16–18], which is inspired by the IEQ approach [19] which in its turn is originated from a Lagrange multiplier approach in [20,21], has proven to be very successful for a large class of gradient flows.

We briefly describe the SAV approach below. To fix the idea, we consider a system with total free energy in the form

$$E(\phi) = \int_\Omega \frac{1}{2} \mathcal{L}\phi \cdot \phi + F(\phi) d\boldsymbol{x}, \tag{1.1}$$

---

* Corresponding author.
E-mail addresses: qcheng4@iit.edu (Q. Cheng), cliu124@iit.edu (C. Liu), shen7@purdue.edu (J. Shen).

where $\mathcal{L}$ is certain linear positive operator. Then a general gradient flow with the above free energy takes the following form

$$\phi_t = -\mathcal{G}\mu,$$
$$\mu = \frac{\delta E(\phi)}{\delta\phi} = \mathcal{L}\phi + F'(\phi),$$

(1.2)

where $\mathcal{G}$ is a positive operator describing the relaxation process of the system.

Assuming $\int_\Omega F(\phi)d\boldsymbol{x} > -C_0$ for some $C_0 > 0$, we introduce a scalar auxiliary variable (SAV) $r(t) = \sqrt{\int_\Omega F(\phi)d\boldsymbol{x} + C_0}$ and rewrite (1.2) as

$$\partial_t\phi = -\mathcal{G}\mu,$$

(1.3)

$$\mu = \mathcal{L}\phi + \frac{r(t)}{\sqrt{\int_\Omega F(\phi)d\boldsymbol{x} + C}}F'(\phi),$$

(1.4)

$$r_t = (\frac{1}{2}\frac{F'(\phi)}{\sqrt{\int_\Omega F(\phi)d\boldsymbol{x} + C}}, \phi_t).$$

(1.5)

The system (1.3)–(1.5), with the initial condition $r(0) = \sqrt{\int_\Omega F(\phi|_{t=0})d\boldsymbol{x} + C_0}$ is equivalent to (1.2). Then, one can construct semi-implicit schemes, by treating the linear terms implicitly and nonlinear terms explicitly in the above, that are unconditionally energy stable schemes and require solving only decoupled linear systems with constant coefficients at each time step. Hence they are very efficient.

However, the unconditional energy stability is with respect to a modified energy

$$\tilde{E}(\phi, r) = \int_\Omega \frac{1}{2}\mathcal{L}\phi \cdot \phi d\boldsymbol{x} + r^2,$$

not the original energy (1.1), and it requires $\int_\Omega F(\phi)d\boldsymbol{x}$ to be bounded from below. A main purpose of this paper is to introduce a new Lagrange multiplier approach which, in addition to the main advantages of the SAV approach, leads to schemes which is unconditionally energy stable with the original energy and does not require the explicitly treated part of the free energy to be bounded from below. Hence, it can be applied to a larger class of gradient flows. The small price we pay for these additional advantages is that we need to solve a nonlinear algebraic equation for the Lagrange multiplier whose cost is negligible compared with the main cost. We present ample numerical evident to show that this new approach is an effective approach for gradient flows.

Another purpose of this paper is to apply the new Lagrange multiplier to an interesting applications, namely, dynamics of block-Copolymers modeled by a coupled Cahn–Hilliard equations [22], and to present simulations, for evolution of frustrated phases of block-Copolymers, which are consistent with experimental observation.

The reminder of this paper is structured as follows. In Section 2, we introduce the new Lagrange multiplier approach for gradient flows, derive its stability property and develop a fast implementation procedure and present numerical results to validate the new approach. In Section 3, we develop the new Lagrange multiplier approach for gradient flows with multiple components. In Section 4, we describe an adaptive time stepping procedure. In Section 5, we use the new approach to simulate evolution of frustrated phases of block-Copolymers. Some concluding remarks are given in Section 6.

2. New Lagrange multiplier approach for gradient flows

We introduce below a new Lagrange multiplier approach for gradient flows.

As in the SAV approach, we introduce a scalar auxiliary function $\eta(t)$, and reformulate the gradient flow (1.2) as

$$\frac{\partial\phi}{\partial t} = -\mathcal{G}\mu,$$
$$\mu = \mathcal{L}\phi + \eta(t)F'(\phi),$$
$$\frac{d}{dt}\int_\Omega F(\phi)d\boldsymbol{x} = \eta(t)\int_\Omega F'(\phi)\phi_t d\boldsymbol{x}.$$

(2.1)

If we set the initial condition for $\eta(t)$ to be $\eta(0) = 1$, then it is easy to see that the new system (2.1) is equivalent to the original system (1.2), i.e., $\eta(t) \equiv 1$ in (2.1).

Note that unlike the SAV approach where $r(t)$ is just an auxiliary variable, the role of $\eta(t)$ here is to serve as a Lagrange multiplier to enforce dissipation of the original energy. Indeed, taking the inner products of the first two equations in the above with μ and $-\phi_t$, respectively, summing up the results together with the third equation, we obtain the original energy dissipative law:

$$\frac{d}{dt}E(\phi) = -(\mu, \mathcal{G}\mu). \tag{2.2}$$

2.1. New schemes, their stability and efficient implementation

Similar to the SAV approach, we can construct efficient and accurate numerical schemes for (2.1). For example, a second order scheme based on Crank–Nicolson is as follows:

$$\frac{\phi^{n+1} - \phi^n}{\delta t} = -\mathcal{G}\mu^{n+\frac{1}{2}}, \tag{2.3}$$

$$\mu^{n+\frac{1}{2}} = \mathcal{L}\phi^{n+\frac{1}{2}} + F'(\phi^{\star,n})\eta^{n+\frac{1}{2}}, \tag{2.4}$$

$$(F(\phi^{n+1}) - F(\phi^n), 1) = \eta^{n+\frac{1}{2}}(F'(\phi^{\star,n}), \phi^{n+1} - \phi^n), \tag{2.5}$$

where $F'(\phi^{\star,n}) = F'(\frac{3}{2}\phi^n - \frac{1}{2}\phi^{n-1})$.

Theorem 2.1. *The Crank–Nicolson scheme* (2.3)–(2.5), *it satisfies the following energy dissipative law,*

$$\frac{E^{n+1} - E^n}{\delta t} = -(\mathcal{G}\mu^{n+\frac{1}{2}}, \mu^{n+\frac{1}{2}}), \tag{2.6}$$

where $E^n = \frac{1}{2}(\mathcal{L}\phi^n, \phi^n) + \int_\Omega F(\phi^n)d\boldsymbol{x}$.

Proof. Taking the inner products of (2.3) with $\mu^{n+\frac{1}{2}}$ and of (2.4) with $-\frac{\phi^{n+1}-\phi^n}{\delta t}$, and multiplying (2.5) with $\frac{1}{\delta t}$, summing up the three relations, we obtain immediately the desired result. $\square$

We now show how to solve scheme (2.3)–(2.5) efficiently. We derive from (2.3)–(2.4) that

$$\frac{\phi^{n+1}}{\delta t} + \mathcal{G}\mathcal{L}\phi^{n+1} = \frac{\phi^n}{\delta t} - \mathcal{G}F'(\phi^{\star,n})\eta^{n+1/2}. \tag{2.7}$$

We define a linear operator χ by

$$\chi(\phi) := (\frac{1}{\delta t}I + \mathcal{G}\mathcal{L})\phi, \tag{2.8}$$

and apply the operator χ^{-1} to both sides of Eq. (2.7) to get

$$\begin{aligned}\phi^{n+1} &= \chi^{-1}\{\frac{\phi^n}{\delta t}\} + \eta^{n+1/2}\chi^{-1}\{-\mathcal{G}F'(\phi^{\star,n})\}\\ &:= p^{n+1} + \eta^{n+1/2}q^{n+1},\end{aligned} \tag{2.9}$$

with p^{n+1} and q^{n+1} being

$$p^{n+1} = \chi^{-1}\{\frac{\phi^n}{\delta t}\}, \quad q^{n+1} = \chi^{-1}\{-\mathcal{G}F'(\phi^{\star,n})\}. \tag{2.10}$$

Now we plug ϕ^{n+1} into Eq. (2.5) to obtain

$$\begin{aligned}&(F(p^{n+1} + \eta^{n+1/2}q^{n+1}) - F(\phi^n), 1)\\ &= \eta^{n+1/2}(F'(\phi^{\star,n}), (p^{n+1} + \eta^{n+1/2}q^{n+1}) - \phi^n).\end{aligned} \tag{2.11}$$

The above equation is a nonlinear algebraic equation for $\eta^{n+1/2}$. The complexity of the nonlinear equation (2.11) depends on $F(\phi)$, e.g., if $F(\phi)$ is the usual double well potential, i.e., $F(\phi) = \frac{1}{4}(\phi^2-1)^2$, (2.11) will be a fourth-order algebraic equation. In general, (2.11) has multiple solutions, but since we are looking for $\eta^{n+1/2}$ as an approximation

to 1, we can use a Newton iteration with 1 as the initial condition, it will generally converge to a solution closer to 1 (assuming δt is not too large).

To summarize, the algorithm consists of the following steps:

Step 1 Compute p^{n+1} and q^{n+1} from (2.10);

Step 2 Find $\eta^{n+1/2}$ by solving (2.11);

Step 3 Set $\phi^{n+1} = p^{n+1} + \eta^{n+1/2}q^{n+1}$, goto the next step.

Note that at each time step, we only need to solve two linear, constant coefficients equations in the **Step 1**, plus a nonlinear algebraic equation in **Step 2**. Since the cost for solving the nonlinear algebraic equation is negligible compared with the cost in **Step 1**, the new algorithm is essentially as efficient as the SAV approach.

Remark 2.1. We note that for the scheme (2.3)–(2.5), the original energy is dissipative, as opposed to the fact that only a modified energy is dissipative in the SAV approach. Furthermore, our new Lagrange multiplier approach does not require the free energy $\int_\Omega F(\phi)dx$ to be bounded from below. On the other hand, the new approach requires solving a nonlinear algebraic equation for the Lagrange multiplier which brings some additional costs and theoretical difficulties for its analysis.

For dissipative systems, it is usually better to use schemes based on backward difference formula (BDF). A second-order scheme for (2.1) based on BDF can be constructed as follows:

$$\frac{3\phi^{n+1} - 4\phi^n + \phi^{n-1}}{2\delta t} = -\mathcal{G}\mu^{n+1}, \tag{2.12}$$

$$\mu^{n+1} = \mathcal{L}\phi^{n+1} + F'(\phi^{\star,n})\eta^{n+1}, \tag{2.13}$$

$$(3F(\phi^{n+1}) - 4F(\phi^n) + F(\phi^{n-1}), 1) = \eta^{n+1}(F'(\phi^{\star,n}), 3\phi^{n+1} - 4\phi^n + \phi^{n-1}), \tag{2.14}$$

where $F'(\phi^{\star,n}) = F'(2\phi^n - \phi^{n-1})$.

Theorem 2.2. *The scheme* (2.12)–(2.14) *satisfies the following energy dissipative law:*

$$\tilde{E}^{n+1} - \tilde{E}^n = -\delta t(\mathcal{G}\mu^{n+1}, \mu^{n+1}) - \frac{1}{4}(\mathcal{L}(\phi^{n+1} - 2\phi^n + \phi^{n-1}), \phi^{n+1} - 2\phi^n + \phi^{n-1}), \tag{2.15}$$

where $\tilde{E}^n = \frac{1}{4}(\mathcal{L}\phi^n, \phi^n) + (\mathcal{L}(2\phi^n - \phi^{n-1}), 2\phi^n - \phi^{n-1}) + \int_\Omega \frac{1}{2}(3F(\phi^n) - F(\phi^{n-1}))dx$.

Proof. Taking the inner product of Eq. (2.12) with μ^{n+1}, we obtain

$$(\frac{3\phi^{n+1} - 4\phi^n + \phi^{n-1}}{2\delta t}, \mu^{n+1}) = -(\mathcal{G}\mu^{n+1}, \mu^{n+1}), \tag{2.16}$$

Taking the inner product of Eq. (2.13) with $3\phi^{n+1} - 4\phi^n + \phi^{n-1}$ and using the identity

$$(2a, 3a - 4b + c) = |a|^2 - |b|^2 + |2a - b|^2 - |2b - c|^2 + |a - 2b + c|^2, \tag{2.17}$$

we obtain

$$\begin{aligned}
(\mu^{n+1}, 3\phi^{n+1} - 4\phi^n + \phi^{n-1}) &= (\mathcal{L}\phi^{n+1}, 3\phi^{n+1} - 4\phi^n + \phi^{n-1}) \\
&+ (F'(\phi^{\star,n})\eta^{n+1}, 3\phi^{n+1} - 4\phi^n + \phi^{n-1}) \\
&= \frac{1}{2}\{(\mathcal{L}\phi^{n+1}, \phi^{n+1}) - (\mathcal{L}\phi^n, \phi^n) + (\mathcal{L}(2\phi^{n+1} - \phi^n), 2\phi^{n+1} - \phi^n) \\
&- (\mathcal{L}(2\phi^n - \phi^{n-1}), 2\phi^n - \phi^{n-1}) + (\mathcal{L}(\phi^{n+1} - 2\phi^n + \phi^{n-1}), \phi^{n+1} - 2\phi^n + \phi^{n-1})\} \\
&+ \eta^{n+1}(F'(\phi^{\star,n}), 3\phi^{n+1} - 4\phi^n + \phi^{n-1}).
\end{aligned} \tag{2.18}$$

Combining (2.16),(2.18) and (2.14), and using

$$3F(\phi^{n+1}) - 4F(\phi^n) + F(\phi^{n-1}) = 3F(\phi^{n+1}) - F(\phi^n) - (3F(\phi^n) - F(\phi^{n-1})),$$

we obtain the desired result. $\quad\square$

Remark 2.2. Note that $\tilde{E}^n$ defined in the above theorem is not exact in the form of original energy. But it is easy to check that $\tilde{E}^n$ is a second-order approximation of $E^n = \frac{1}{2}(\mathcal{L}\phi^n, \phi^n) + \int_\Omega F(\phi^n)d\boldsymbol{x}$.

2.2. A modified version

a second order scheme based on Crank–Nicolson is as follows:

$$\frac{\phi^{n+1} - \phi^n}{\delta t} = -\mathcal{G}\mu^{n+\frac{1}{2}}, \tag{2.19}$$

$$\mu^{n+\frac{1}{2}} = \mathcal{L}\phi^{n+\frac{1}{2}} + F'(\phi^{\star,n})\eta^{n+\frac{1}{2}}, \tag{2.20}$$

$$(F(\bar{\phi}^{n+1}) - F(\bar{\phi}^n), 1) = \eta^{n+\frac{1}{2}}(F'(\phi^{\star,n}), \phi^{n+1} - \phi^n), \tag{2.21}$$

where $F'(\phi^{\star,n}) = F'(\frac{3}{2}\phi^n - \frac{1}{2}\phi^{n-1})$ and $\bar{\phi}^{n+1} = p^{n+1} + q^{n+1}$ with p^{n+1}, q^{n+1} being defined in (2.10).

The above scheme can be implemented in essentially the same fashion as the scheme (2.3)–(2.5), except that $\eta^{n+\frac{1}{2}}$ can now be determined explicitly without using a Newton iteration, see the remark below.

Remark 2.3. Since it is expected that $\eta^{n+\frac{1}{2}}$ approaches the exact solution $\eta(t) \equiv 1$, we replaced $\eta^{n+\frac{1}{2}}$ by 1 in the definition of $\bar{\phi}^{n+1}$. Consequently, we can determine $\eta^{n+\frac{1}{2}}$ explicitly from (2.21), namely,

$$\eta^{n+\frac{1}{2}} = \frac{-(F'(\phi^{\star,n}), p^{n+1} - \phi^n) \pm \sqrt{(F'(\phi^{\star,n}), p^{n+1} - \phi^n)^2 + 4(F'(\phi^{\star,n}), q^{n+1})(F(\bar{\phi}^{n+1}) - F(\bar{\phi}^n), 1)}}{2(F'(\phi^{\star,n}), q^{n+1})}. \tag{2.22}$$

We can easily establish the following result:

Theorem 2.3. *The modified Crank–Nicolson scheme* (2.19)–(2.21) *satisfies the following energy dissipative law,*

$$\frac{\hat{E}^{n+1} - \hat{E}^n}{\delta t} = -(\mathcal{G}\mu^{n+\frac{1}{2}}, \mu^{n+\frac{1}{2}}), \tag{2.23}$$

where $\hat{E}^n = \frac{1}{2}(\mathcal{L}\phi^n, \phi^n) + \int_\Omega F(\bar{\phi}^n)d\boldsymbol{x}$.

2.3. Numerical validations

We provide below some numerical tests to validate our new schemes.

2.3.1. Accuracy test

In this subsection, in order to test accuracy and convergence rate of scheme BDF2 and Crank–Nicolson in time. We consider the Allen–Cahn ($\mathcal{G} = I$) and Cahn–Hillard equation ($\mathcal{G} = -\Delta$) in the form

$$\phi_t = -\mathcal{G}\mu + f,$$
$$\mu = -\Delta\phi + \frac{1}{\epsilon^2}\phi(\phi^2 - 1), \tag{2.24}$$

with periodic boundary conditions. We choose a force function f such that the exact solution is

$$\phi(x, y) = (\frac{\sin(2x)\cos(2y)}{4} + 0.48)(1 - \frac{\sin^2(t)}{2}),$$

and use 128^2 Fourier-spectral modes in space so that the error is dominated by the time discretization error. In Table 1 and Table 2, we present L^∞ errors for both Allen–Cahn and Cahn–Hilliard equations at various time steps. It is observed that both scheme BDF2 and CN achieve second order convergence rate in time (see Table 2).

Next we examine the energy stability. We take $f = 0$ in domain $[0, 2\pi)^2$ and start with a random initial condition

$$\phi(x, y) = 0.03 + 0.001\,\text{rand}(x, y),$$

where $\text{rand}(x, y)$ represents random data between $[-1, 1]^2$. The energy curves are plotted for both Allen–Cahn equation and Cahn–Hilliard equation with $\epsilon^2 = 0.005$ in Fig. 1. It is observed from this figure that the computed energy for both cases decays with time.

Table 1
Accuracy test: with given exact solution for Allen–Cahn equation and $\epsilon^2 = 0.02$. The L^∞ errors at $t = 0.1$ for the phase variables ϕ computed by scheme BDF2 and Crank–Nicolson using various time steps.

δt	$BDF2$	Order	CN	Order
2×10^{-3}	$1.11E(-5)$	–	$5.31E(-6)$	–
1×10^{-3}	$2.88E(-6)$	1.94	$1.38E(-6)$	1.95
5×10^{-4}	$7.31E(-7)$	1.95	$3.57E(-7)$	1.98
2.5×10^{-4}	$1.85E(-7)$	1.95	$9.23E(-8)$	1.98
1.25×10^{-4}	$4.64E(-8)$	1.99	$2.32E(-8)$	1.99
6.25×10^{-5}	$1.17E(-8)$	1.98	$5.86E(-9)$	1.91
3.125×10^{-5}	$2.93E(-9)$	2.00	$1.46E(-9)$	2.00

Table 2
Accuracy test: with given exact solution for Cahn–Hilliard equation and $\epsilon^2 = 0.06$. The L^∞ errors at $t = 0.1$ for the phase variables ϕ computed by scheme BDF2 and Crank–Nicolson using various time steps.

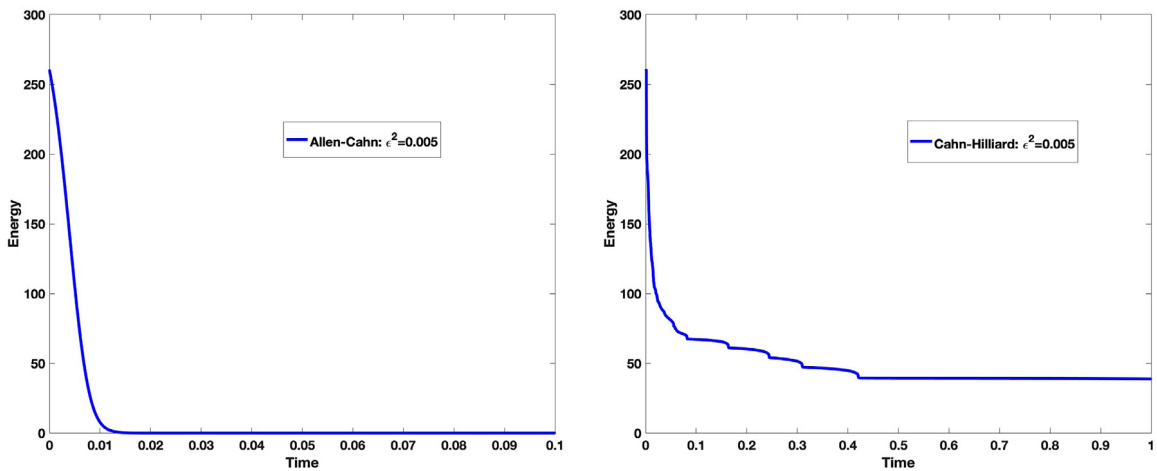| δt	$BDF2$	Order	CN	Order
2×10^{-3}	$2.75E(-6)$	–	$3.04E(-6)$	–
1×10^{-3}	$6.92E(-7)$	1.99	$7.67E(-7)$	1.98
5×10^{-4}	$1.73E(-7)$	2.00	$1.92E(-7)$	1.99
2.5×10^{-4}	$4.36E(-8)$	1.98	$4.83E(-8)$	1.99
1.25×10^{-4}	$1.09E(-9)$	2.00	$1.20E(-8)$	2.00
6.25×10^{-5}	$2.72E(-9)$	2.00	$3.02E(-9)$	1.99
3.125×10^{-5}	$6.80E(-10)$	2.00	$7.57E(-10)$	2.00

Fig. 1. Energy evolution of Allen–Cahn and Cahn–Hilliard equations by using Scheme BDF2 of new Lagrange multiplier approach with time step $\delta t = 10^{-5}$.

2.3.2. Molecular beam epitaxial without slope selection

As an example where the nonlinear functional is unbounded from below, we consider a model for molecular beam epitaxial (MBE) without slope selection [23]. For this model, the total free energy is $E(\phi) = \int_\Omega \frac{\epsilon^2}{2}|\Delta\phi|^2 + F(\phi)dx$, where the nonlinear potential is

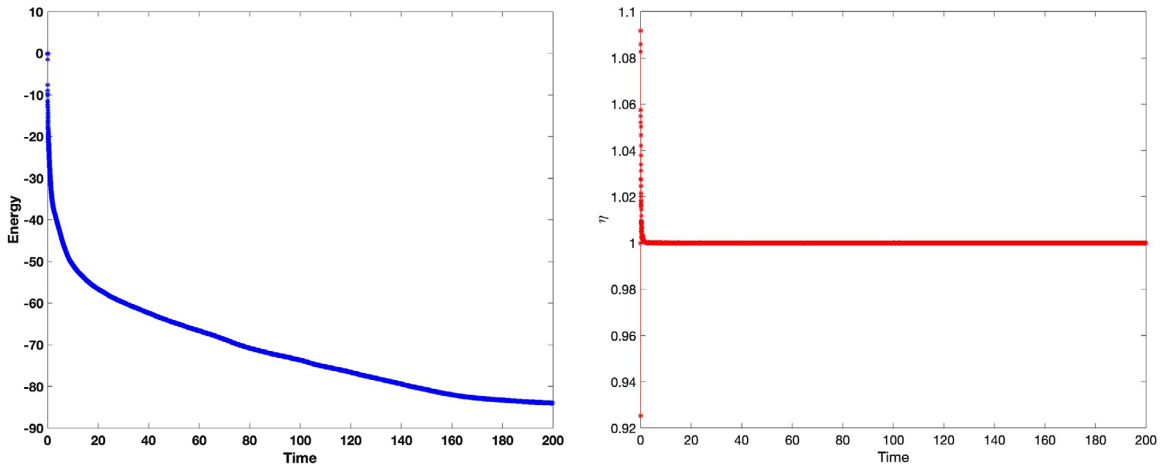$$F(\phi) = -\frac{1}{2}\ln(1 + |\nabla\phi|^2). \tag{2.25}$$

Fig. 2. The evolution of energy and η with time for MBE model without slope selection.

Since the Logarithmic potential is not bounded from below, one has to use a different energy splitting so that the SAV approach can be applied [24]. However, our new approach can be directly applied since there is no requirement of boundedness from below. More precisely, the L^2 gradient flow with respect to the free energy above is

$$\phi_t = -M\frac{\delta E(\phi)}{\delta \phi} = -M\big(\epsilon^2 \Delta^2 \phi + F'(\phi)\big), \tag{2.26}$$

with boundary conditions:

$$(i)\ \phi \text{ is periodic with or } (ii)\ \partial_{\boldsymbol{n}}\phi|_{\partial\Omega} = \partial_{\boldsymbol{n}}\Delta\phi|_{\partial\Omega} = 0, \tag{2.27}$$

where $\boldsymbol{n}$ is the unit outward normal on the boundary $\partial\Omega$. In the above, M is a mobility constant, and $F'(\phi) = \nabla \cdot \left(\frac{\nabla \phi}{1+|\nabla\phi|^2}\right)$.

Then, a second-order scheme based on the new Lagrange multiplier approach is:

$$\frac{3\phi^{n+1} - 4\phi^n + \phi^{n-1}}{2\delta t} + M\big(\epsilon^2 \Delta^2 \phi^{n+1} + \eta^{n+1} F'(\phi^{\star,n})\big) = 0, \tag{2.28}$$

$$\eta^{n+1}(F'(\phi^{\star,n}), 3\phi^{n+1} - 4\phi^n + \phi^{n-1}) = (3F(\nabla\phi^{n+1}) - 4F(\nabla\phi^n) + F(\nabla\phi^{n-1}), 1). \tag{2.29}$$

Similarly as in the proof of Theorem 2.2, we can easily show that the above equation is unconditionally energy stable. It is also clear that it can also be efficiently implemented.

We present in Fig. 2 the time evolutions of total energy and the Lagrange multiplier in domain $[0, 2\pi]^2$. The initial condition is taken as a randomly perturbed concentration field as follows:

$$\phi(t = 0) = 0.01 \operatorname{rand}(x, y), \tag{2.30}$$

where the $\operatorname{rand}(x, y)$ is a uniformly distributed random function in $[-1, 1]^2$. One observes that the total energy decays monotonically and that the values of the Lagrange multiplier are essentially one except at a few initial steps. An example of the coarsening process is shown in Fig. 3.

3. Gradient flows with multiple components

As the SAV approach, the new Lagrange multiplier approach can be applied to gradient flows with multiple components. As a particular example, we consider the following coupled non-local Cahn–Hilliard type system:

$$u_t = M_u \Delta \mu_u, \tag{3.1}$$

$$\mu_u = -\epsilon_u^2 \Delta u + (u^2 - 1)u + \alpha v + \beta v^2 + 2\gamma uv, \tag{3.2}$$
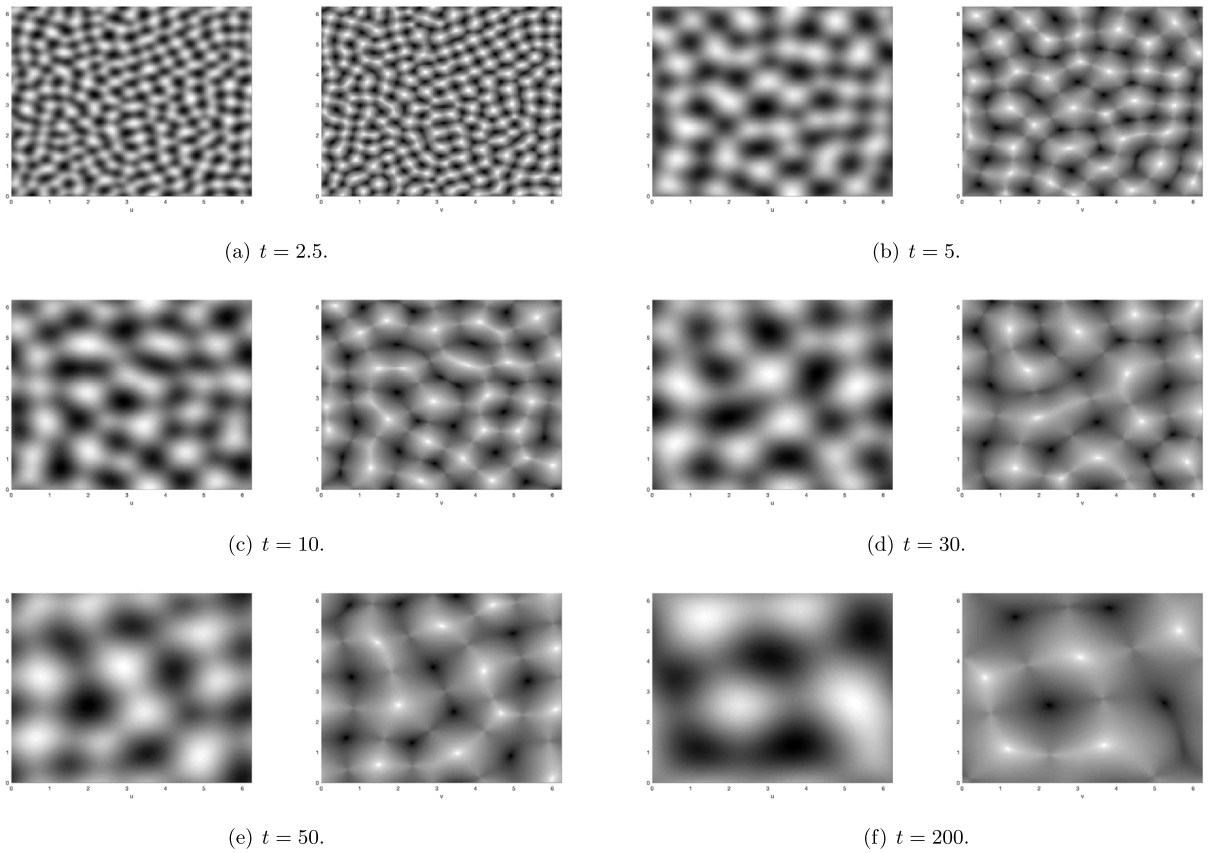
$$v_t = M_v \Delta \mu_v, \tag{3.3}$$

(a) $t = 2.5$.

(b) $t = 5$.

(c) $t = 10$.

(d) $t = 30$.

(e) $t = 50$.

(f) $t = 200$.

Fig. 3. The isolines of the numerical solutions of the height function ϕ and its Laplacian $\Delta\phi$ for the model without slope selection with random initial condition. For each subfigure, the left is ϕ and the right is $\Delta\phi$. Snapshots are taken at $t = 2.5, 5, 10, 30, 50, 200$, respectively.

$$\mu_v = -\epsilon_v^2 \Delta v + (v^2 - 1)v + \alpha u + 2\beta uv + \gamma u^2 - \sigma \Delta^{-1}(v - \overline{v}), \tag{3.4}$$

with boundary conditions

$$(i) \text{ periodic; or } (ii) \ \partial_{\mathbf{n}} u|_{\partial\Omega} = \partial_{\mathbf{n}} \Delta u|_{\partial\Omega} = \partial_{\mathbf{n}} v|_{\partial\Omega} = \partial_{\mathbf{n}} \Delta v|_{\partial\Omega} = 0. \tag{3.5}$$

The above system is introduced in [22] to model a blend of homopolymer and copolymer components. We defer the physical description about the system to Section 5, and consider how to apply the new Lagrange multiplier approach to solve it efficiently.

The system (3.1)–(3.4) can be interpreted as a gradient flow as follows

$$u_t = M_u \Delta \frac{\delta E(u, v)}{\delta u}, \tag{3.6}$$

$$v_t = M_v \Delta \frac{\delta E(u, v)}{\delta v}, \tag{3.7}$$

with the total free energy

$$E(u, v) = \int_\Omega \frac{\epsilon_u^2}{2} |\nabla u|^2 + \frac{\epsilon_v^2}{2} |\nabla v|^2 + W(u, v) + \frac{\sigma}{2} \left| (-\Delta)^{-\frac{1}{2}}(v - \overline{v}) \right|^2 d\mathbf{x}, \tag{3.8}$$

where

$$W(u, v) = \frac{(u^2 - 1)^2}{4} + \frac{(v^2 - 1)^2}{4} + \alpha uv + \beta uv^2 + \gamma u^2 v. \tag{3.9}$$

Indeed, one can easily check that

$$\frac{\delta E(u,v)}{\delta u} = -\epsilon_u^2 \Delta u + \frac{\delta W}{\delta u} = \mu_u, \quad \frac{\delta E(u,v)}{\delta v} = -\epsilon_u^2 \Delta v + \frac{\delta W}{\delta v} - \sigma \Delta^{-1}(v - \overline{v}) = \mu_v.$$

3.1. New schemes based on the Lagrange multiplier approach

We introduce a Lagrange multiplier $\eta(t)$ and rewrite (3.6)–(3.7) as

$$u_t = M_u \Delta \mu_u, \tag{3.10}$$

$$\mu_u = -\epsilon_u^2 \Delta u + \frac{\delta W}{\delta u}\eta(t), \tag{3.11}$$

$$v_t = M_v \Delta \mu_v, \tag{3.12}$$

$$\mu_v = -\epsilon_u^2 \Delta v + \frac{\delta W}{\delta v}\eta(t) - \sigma \Delta^{-1}(v - \overline{v}), \tag{3.13}$$

$$\frac{d}{dt}\int_\Omega W(u,v)d\boldsymbol{x} = \eta(t)\int_\Omega (\frac{\delta W}{\delta u}u_t + \frac{\delta W}{\delta v}v_t)d\boldsymbol{x}. \tag{3.14}$$

Taking the inner products of (3.10)–(3.13) with μ_u, u_t, μ_v, v_t, respectively, summing up the results along with (3.14), we obtain the energy dissipation law

$$\frac{d}{dt}E(u,v) = -M_u(\nabla\mu_u, \nabla\mu_u) - M_v(\nabla\mu_v, \nabla\mu_v).$$

As in the previous section, we can construct a second-order scheme for the above system as follows: assuming that u^{n-1}, u^n and v^{n-1}, v^n are known, we find u^{n+1} and v^{n+1} as follows:

$$\frac{3u^{n+1} - 4u^n + u^{n-1}}{2\delta t} = M_u \Delta \mu_u^{n+1}, \tag{3.15}$$

$$\mu_u^{n+1} = -\epsilon_u^2 \Delta u^{n+1} + (\frac{\delta W}{\delta u})^{\star,n}\eta^{n+1}, \tag{3.16}$$

$$\frac{3v^{n+1} - 4v^n + v^{n-1}}{2\delta t} = M_v \Delta \mu_v^{n+1}, \tag{3.17}$$

$$\mu_v^{n+1} = -\epsilon_v^2 \Delta v^{n+1} + (\frac{\delta W}{\delta v})^{\star,n}\eta^{n+1} - \sigma \Delta^{-1}(v^{n+1} - \overline{v}), \tag{3.18}$$

$$(3W(u^{n+1}, v^{n+1}) - 4W(u^n, v^n) + W(u^{n-1}, v^{n-1}), 1) \tag{3.19}$$
$$= \eta^{n+1}\{((\frac{\delta W}{\delta u})^{\star,n}, 3u^{n+1} - 4u^n + u^{n-1}) + ((\frac{\delta W}{\delta v})^{\star,n}, 3v^{n+1} - 4v^n + v^{n-1})\},$$

where $f^{\star,n} = 2f^n - f^{n-1}$ for any function f, and the boundary conditions are given by (3.5).

Theorem 3.1. *The numerical scheme* (3.15)–(3.19) *is unconditional energy stable in the sense that*

$$\frac{E^{n+1} - E^n}{\delta t} \le -(M_u\|\nabla\mu_u^{n+1}\| + M_v\|\nabla\mu_v^{n+1}\|^2), \tag{3.20}$$

where

$$E^{n+1} = \int_\Omega \frac{\epsilon_u^2}{2}|\nabla u^{n+1}|^2 + \frac{\epsilon_v^2}{2}|\nabla v^{n+1}|2 + \frac{1}{2}\big(3W(u^{n+1}, v^{n+1}) - W(u^n, v^n)\big)$$
$$+ \frac{\sigma}{2}|(-\Delta)^{-\frac{1}{2}}(v^{n+1} - \overline{v}^{n+1})|^2 d\boldsymbol{x}.$$

Proof. Taking the inner products of (3.15) and (3.17) with μ_u^{n+1} and μ_v^{n+1}, respectively, we find

$$(\frac{3u^{n+1} - 4u^n + u^{n-1}}{2\delta t}, \mu_u^{n+1}) = -M_u\|\nabla\mu_u^{n+1}\|^2, \tag{3.21}$$

$$(\frac{3v^{n+1} - 4v^n + v^{n-1}}{2\delta t}, \mu_v^{n+1}) = -M_v\|\nabla\mu_v^{n+1}\|^2. \tag{3.22}$$

Taking the inner products of (3.16) and (3.18) with $3u^{n+1} - 4u^n + u^{n-1}$ and $3v^{n+1} - 4v^n + v^{n-1}$, respectively, and using the identity (2.17), we find

$$
\begin{aligned}
(\mu_u^{n+1}, 3u^{n+1} - 4u^n + u^{n-1}) &= \frac{\epsilon_u^2}{2}\{(\|\nabla u^{n+1}\|^2 - \|2\nabla u^{n+1} - \nabla u^n\|^2) \\
&- (\|\nabla u^n\|^2 - \|2\nabla u^n - \nabla u^{n-1}\|^2) + \|\nabla u^{n+1} - 2\nabla u^n + \nabla u^{n-1}\|^2\} \\
&+ ((\frac{\delta W}{\delta u})^{\star,n}\eta^{n+1}, 3u^{n+1} - 4u^n + u^{n-1}),
\end{aligned}
$$

and

$$
\begin{aligned}
(\mu_v^{n+1}, 3v^{n+1} - 4v^n + v^{n-1}) &= \frac{\epsilon_v^2}{2}\{(\|\nabla v^{n+1}\|^2 - \|2\nabla v^{n+1} - \nabla v^n\|^2) \\
&- (\|\nabla v^n\|^2 - \|2\nabla v^n - \nabla v^{n-1}\|^2) + \|\nabla v^{n+1} - 2\nabla v^n + \nabla v^{n-1}\|^2\} \\
&+ ((\frac{\delta W}{\delta v})^{\star,n}\eta^{n+1}, 3v^{n+1} - 4v^n + v^{n-1}).
\end{aligned}
$$

Combing the above relations and using (3.19), we obtain the desired result. □

Next, we describe how to solve this coupled system (3.15)–(3.19) efficiently. We first eliminate μ_u and μ_v to rewrite Eqs. (3.15)–(3.16) and (3.17)–(3.18) as

$$
\frac{3u^{n+1}}{2\delta t} + M_u\epsilon_u^2\Delta^2 u^{n+1} = \frac{4u^n - u^{n-1}}{2\delta t} + M_u\Delta(\frac{\delta W}{\delta u})^{\star,n}\eta^{n+1}, \tag{3.23}
$$

$$
\frac{3v^{n+1}}{2\delta t} + M_v\epsilon_v^2\Delta^2 v^{n+1} = \frac{4v^n - v^{n-1}}{2\delta t} + M_v\Delta(\frac{\delta W}{\delta v})^{\star,n}\eta^{n+1}. \tag{3.24}
$$

Define two linear operators

$$
\chi_u u := (\frac{3}{2\delta t} + M_u\epsilon_u^2\Delta^2)u, \quad \chi_v v := (\frac{3}{2\delta t} + M_v\epsilon_v^2\Delta^2)v,
$$

with boundary conditions specified in (3.5), and apply χ_u^{-1} and χ_v^{-1} to Eqs. (3.23) and (3.24), respectively, we obtain

$$
\begin{aligned}
u^{n+1} &= \chi_u^{-1}\{\frac{4u^n - u^{n-1}}{2\delta t} + M_u\Delta(\frac{\delta W}{\delta u})^{\star,n}\eta^{n+1}\}. \\
&:= p_u^n + \eta^{n+1}q_u^n,
\end{aligned} \tag{3.25}
$$

$$
\begin{aligned}
v^{n+1} &= \chi_v^{-1}\{\frac{4v^n - v^{n-1}}{2\delta t} + M_v\Delta(\frac{\delta W}{\delta v})^{\star,n}\eta^{n+1}\} \\
&:= p_v^n + \eta^{n+1}q_v^n.
\end{aligned} \tag{3.26}
$$

where

$$
\begin{aligned}
p_u^n &= \chi_u^{-1}\{\frac{4u^n - u^{n-1}}{2\delta t}\}, \quad q_u^n = \chi_u^{-1}\{M_u\Delta(\frac{\delta W}{\delta u})^{\star,n}\}, \\
p_v^n &= \chi_v^{-1}\{\frac{4v^n - v^{n-1}}{2\delta t}\}, \quad q_v^n = \chi_v^{-1}\{M_v\Delta(\frac{\delta W}{\delta v})^{\star,n}\}.
\end{aligned} \tag{3.27}
$$

Then plugging u^{n+1} and v^{n+1} in (3.25)–(3.26) into (3.19), we obtain a nonlinear algebraic equation for η^{n+1}:

$$
\begin{aligned}
&(\frac{\delta W}{\delta u})^{\star,n}\eta^{n+1}, 3(p_u^n + \eta^{n+1}q_u^n) + ((\frac{\delta W}{\delta v})^{\star,n}\eta^{n+1}, 3(p_v^n + \eta^{n+1}q_v^n)) \\
&- (3W(p_u^n + \eta^{n+1}q_u^n, p_v^n + \eta^{n+1}q_v^n), 1) = g^{\star,n},
\end{aligned} \tag{3.28}
$$

where $g^{\star,n}$ represents all known explicit terms.

Since $W(u, v)$ is a polynomial of degree four for u and v, we find that (3.28) is a nonlinear algebraic equation of degree four for η^{n+1}, which can be easily solved by using a Newton iteration with 1 as the initial condition. To summarize, the new Lagrange multiplier algorithm for the coupled Cahn–Hilliard system consists of the following steps:

Table 3
Accuracy test: with given exact solution for the coupled model (3.1)-(3.4). The L^∞ errors at $t = 0.1$ for the phase variables u and v computed by the scheme based on BDF2 using various time steps.

δt	u	Order	v	Order
4×10^{-3}	$9.87E(-6)$	–	$8.29E(-6)$	–
2×10^{-3}	$2.46E(-6)$	2.00	$2.07E(-6)$	2.00
1×10^{-3}	$6.16E(-7)$	1.99	$5.17E(-7)$	2.00
5×10^{-4}	$1.54E(-7)$	2.00	$1.29E(-7)$	2.00
2.5×10^{-4}	$3.85E(-8)$	1.99	$3.23E(-8)$	1.99
1.25×10^{-4}	$9.63E(-9)$	1.99	$8.07E(-9)$	1.99
6.25×10^{-5}	$2.40E(-9)$	2.00	$2.01E(-9)$	2.00

Table 4
Accuracy test: with given exact solution for the coupled model (3.1)-(3.4). The L^∞ errors at $t = 0.1$ for the phase variables u and v computed by the scheme based on Crank–Nicolson using various time steps.

δt	u	Order	v	Order
4×10^{-3}	$3.69E(-6)$	–	$3.03E(-6)$	–
2×10^{-3}	$9.80E(-7)$	1.91	$8.01E(-7)$	1.92
1×10^{-3}	$2.50E(-7)$	1.97	$2.04E(-7)$	1.97
5×10^{-4}	$6.32E(-8)$	1.98	$5.15E(-8)$	1.98
2.5×10^{-4}	$1.60E(-8)$	1.98	$1.30E(-8)$	1.98
1.25×10^{-4}	$3.98E(-9)$	2.00	$3.24E(-9)$	2.00
6.25×10^{-5}	$9.34E(-10)$	2.09	$7.77E(-10)$	2.00

Step 1 Compute p_u^n, q_u^n, p_v^n and q_v^n from (3.27);

Step 2 Solve equation (3.28) to obtain η^{n+1};

Step 3 Update u^{n+1} and v^{n+1} with (3.23) and (3.24), and goto the next step.

The main cost of the scheme (3.15)–(3.19) at each time step is in **Step 1** where one needs to solve four linear, constant coefficient fourth-order equations. Hence, the scheme is very efficient.

3.2. Numerical validations

We will first present some numerical results to validate the stability and the accuracy of the scheme (3.15)–(3.19) using a Fourier spectral method with 128^2 modes in the spatial domain $\Omega = [0, 2\pi)^2$.

We first test the accuracy with a manufactured exact solution given by

$$u(x, y, t) = (\frac{\sin(2x)\sin(2y)}{4} + 0.48)(1 - \frac{\sin^2(t)}{2}),$$

$$v(x, y, t) = (\frac{\sin(2x)\sin(2y)}{4} + 0.48)(1 - \frac{\sin^2(t)}{2}).$$

We set the parameters to be

$$\epsilon_u = 0.075 \quad \epsilon_v = 0.075 \quad \sigma = 10 \quad \alpha = -0.1 \quad \beta = -0.1 \quad \gamma = 0.$$

In Tables 3 and 4, we list the L^∞ errors at $t = 0.1$ of phase variables u and v with various time steps by using new schemes based on BDF2 and Crank–Nicolson. We observe that both schemes have second-order convergence rate in time.

Next, we examine the energy dissipation and accuracy using a realistic simulation. Since excessively small time steps may be needed to obtain accurate results using the scheme (3.15)–(3.19), we construct a "stabilized" version
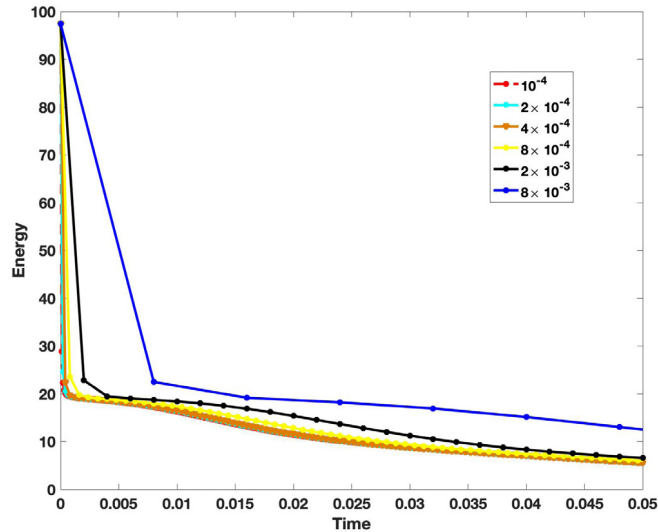
Fig. 4. Evolution of the free energy using the stabilized scheme with various time steps.

based on the following splitting of free energy:

$$
E(u, v) = \int_\Omega \frac{\epsilon_u^2}{2}|\nabla u|^2 + \frac{\epsilon_v^2}{2}|\nabla v|^2 + \frac{S_u}{2}|u|^2 + \frac{S_v}{2}|v|^2 \boldsymbol{x}
$$
$$
+ \int_\Omega W(u, v) - \frac{S_u}{2}|u|^2 - \frac{S_v}{2}|v|^2 + \frac{\sigma}{2}\left|(-\Delta)^{-\frac{1}{2}}(v - \overline{v})\right|^2 d\boldsymbol{x},
$$
(3.29)

where $W(u, v)$ is given in (3.9) and $S_u, S_v \geq 0$ are stabilizing constants.

Setting $\tilde{W}(u, v) = W(u, v) - \frac{S_u}{2}|u|^2 - \frac{S_v}{2}|v|^2$, the "stabilized" version of the scheme (3.15)–(3.19) corresponding to the above splitting is:

$$
\frac{3u^{n+1} - 4u^n + u^{n-1}}{2\delta t} = M_u \Delta \mu_u^{n+1},
$$
(3.30)

$$
\mu_u^{n+1} = -\epsilon_u^2 \Delta u^{n+1} + S_u u^{n+1} + (\frac{\delta \tilde{W}}{\delta u})^{\star,n} \eta^{n+1},
$$
(3.31)

$$
\frac{3v^{n+1} - 4v^n + v^{n-1}}{2\delta t} = M_v \Delta \mu_v^{n+1},
$$
(3.32)

$$
\mu_v^{n+1} = -\epsilon_v^2 \Delta v^{n+1} + S_v v^{n+1} + (\frac{\delta \tilde{W}}{\delta v})^{\star,n} \eta^{n+1} - \sigma \Delta^{-1}(v^{n+1} - \overline{v}),
$$
(3.33)

$$
(3\tilde{W}(u^{n+1}, v^{n+1}) - 4\tilde{W}(u^n, v^n) + \tilde{W}(u^{n-1}, v^{n-1}), 1)
$$
(3.34)
$$
= \eta^{n+1}\{((\frac{\delta \tilde{W}}{\delta u})^{\star,n}, 3u^{n+1} - 4u^n + u^{n-1}) + ((\frac{\delta \tilde{W}}{\delta v})^{\star,n}, 3v^{n+1} - 4v^n + v^{n-1})\}.
$$

Obviously, we can prove that the above scheme is also unconditionally energy stable as in Theorem 2.2, and can be efficiently implemented as the scheme (3.15)–(3.19). Note that the choice of stabilized constants does not affect the energy stability but it does impact on the accuracy, so its choice is a delicate matter: being too small will not provide enough stabilization while being too large will lead to over dissipation.

We take uniformly distributed random functions in $[-1, 1]^2$ with zero mean as initial conditions, and set the parameters to be

$$
\epsilon_u = 0.05 \quad \epsilon_v = 0.05 \quad \sigma = 10 \quad \alpha = -0.1 \quad \beta = 0.75 \quad \gamma = 0,
$$
(3.35)

and the stabilized constants are $S_u = S_v = 1$.

We plot in Fig. 4 evolution of the total energy computed with different time steps. We observe that all energies decay with time as expected. For $\delta t = 8 \times 10^{-4}, 4 \times 10^{-4}, 2 \times 10^{-4}, 10^{-4}$, the four energy curves essentially coincide. However, significant differences appear with $\delta t = 2 \times 10^{-3}$ and $\delta t = 8 \times 10^{-3}$. So in order to achieve

good accuracy for numerical simulations, we should choose $\delta t \leq 8 \times 10^{-4}$. Note that the required time step would be much smaller without the stabilization, i.e., $S_u = S_v = 0$.

4. Adaptive time stepping

A main advantage of unconditional energy stable numerical schemes is that one can combine them with an adaptive time stepping so that their efficiency can be further improved. This has been demonstrated with many examples for the SAV approach [17]. We can also combine an adaptive time stepping strategy with the new Lagrange multiplier approach.

Since it is more difficult to devise an adaptive time stepping for the scheme based on BDF2, we construct below a second-order scheme with variable time steps based on a second-order Crank–Nicolson scheme. To fix the idea, we take the coupled problem (3.1)–(3.4) as an example.

A stabilized second-order Crank–Nicolson scheme with variable time step is as follows: assuming that u^{n-1}, u^n and v^{n-1}, v^n are known, set $a_n = \frac{\delta t_n}{\delta t_{n-1}}$ and $\delta t_n = t^{n+1} - t^n$, we solve u^{n+1} and v^{n+1} as follows:

$$\frac{u^{n+1} - u^n}{\delta t_n} = M_u \Delta \mu_u^{n+\frac{1}{2}}, \tag{4.1}$$

$$\mu_u^{n+\frac{1}{2}} = -\epsilon_u^2 \Delta u^{n+\frac{1}{2}} + S_u u^{n+\frac{1}{2}} + (\frac{\delta \tilde{W}}{\delta u})^{\star,n} \eta^{n+\frac{1}{2}}, \tag{4.2}$$

$$\frac{v^{n+1} - v^n}{\delta t_n} = M_v \Delta \mu_v^{n+\frac{1}{2}}, \tag{4.3}$$

$$\mu_v^{n+\frac{1}{2}} = -\epsilon_v^2 \Delta v^{n+\frac{1}{2}} + S_v v^{n+\frac{1}{2}} + (\frac{\delta \tilde{W}}{\delta v})^{\star,n} \eta^{n+\frac{1}{2}} - \sigma \Delta^{-1}(v^{n+\frac{1}{2}} - \overline{v}), \tag{4.4}$$

$$\eta^{n+\frac{1}{2}}((\frac{\delta \tilde{W}}{\delta u})^{\star,n}, u^{n+1} - u^n) + ((\frac{\delta \tilde{W}}{\delta v})^{\star,n}, v^{n+1} - v^n)$$
$$= (\tilde{W}(u^{n+1}, v^{n+1}) - \tilde{W}(u^n, v^n), 1), \tag{4.5}$$

where $f^{n+\frac{1}{2}} = \frac{1}{2}(f^{n+1} + f^n)$ and $f^{\star,n} = (1 + \frac{a_n}{2})f^n - \frac{a_n}{2}f^{n-1}$ for any function f.

The above scheme can also be efficiently implemented as the scheme (3.15)–(3.19), and the following result can be easily established.

Theorem 4.1. *The scheme* (4.1)–(4.5) *is unconditional energy stable in the sense that*

$$\frac{E^{n+1} - E^n}{\delta t_n} = -(M_u \|\nabla \mu_u^{n+\frac{1}{2}}\|^2 + M_v \|\nabla \mu_v^{n+\frac{1}{2}}\|^2), \tag{4.6}$$

where $E^{n+1} = \int_\Omega \frac{\epsilon_u^2}{2}|\nabla u^{n+1}|^2 + \frac{\epsilon_v^2}{2}|\nabla v^{n+1}|^2 + W(u^{n+1}, v^{n+1}) + \frac{\sigma}{2}|(-\Delta)^{-\frac{1}{2}}(v^{n+1} - \overline{v}^{n+1})|^2 d\boldsymbol{x}$.

Then we use the following algorithm to choose time steps adaptively.

Algorithm for adaptive time stepping:

    Given Solutions at time steps n and $n - 1$; parameters *tol* and ρ, and the preassigned minimum and maximin allowable time steps $\delta t_{\min}$ and $\delta t_{\max}$.

    Step 1: Compute u_1^{n+1}, v_1^{n+1} by a first-order Lagrange multiplier scheme with δt_n.

    Step 2: Compute u_2^{n+1}, v_2^{n+1} by adaptive Crank–Nicolson scheme (4.1)–(4.5) with δt_n.

    Step 3: Calculate $e_{n+1} = \max\{\frac{\|u_2^{n+1} - u_1^{n+1}\|}{\|u_2^{n+1}\|}, \frac{\|v_2^{n+1} - v_1^{n+1}\|}{\|v_2^{n+1}\|}\}$.

    Step 4: if $e_{n+1} > tol$, **then**

        Recalculate time step $\delta t_n \leftarrow \max\{\delta t_{\min}, \min\{A_{dp}(e_{n+1}, \delta t_n), \delta t_{\max}\}\}$.

    Step 5: goto Step 1

    Step 6: else

        Update time step $\delta t_{n+1} \leftarrow \max\{\delta t_{\min}, \min\{A_{dp}(e_{n+1}, \delta t_n), \delta t_{\max}\}\}$,
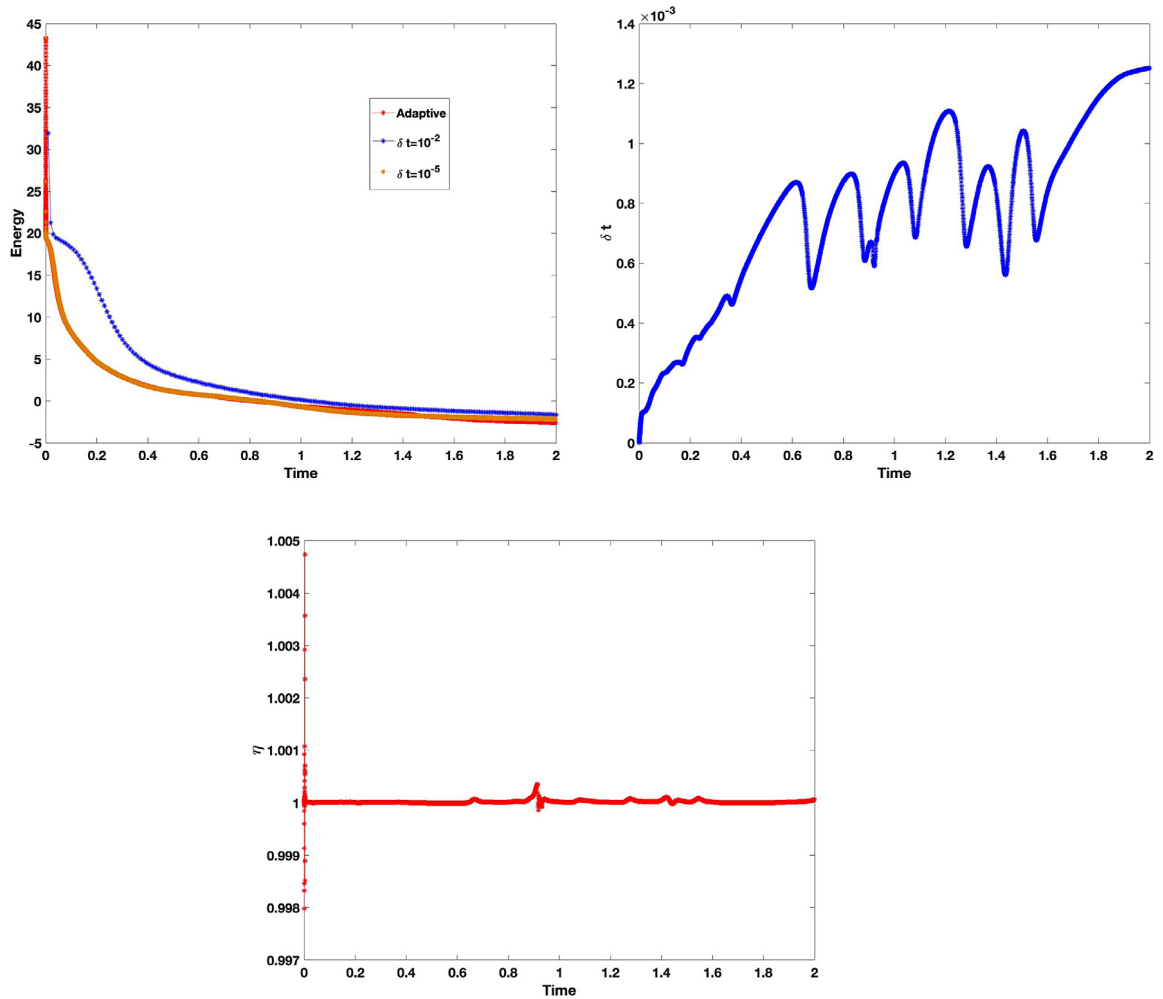
    Step 7: endif

Fig. 5. First: evolution of the free energy with uniform time steps and adaptive time stepping; Second: evolution of the time steps with adaptive time stepping; Third: evolution of the Lagrange multiplier η with adaptive time stepping.

where $A_{dp}(e, \tau)$ is a suitable function, e.g., [25,26]:

$$A_{dp}(e, \tau) = \rho(\frac{tol}{e})^{\frac{1}{2}}\tau. \tag{4.7}$$

As an example, we used the above adaptive scheme with $S_u = S_v = 5$ to solve the coupled Cahn–Hilliard equations with the following parameters

$$\epsilon_u = 0.075 \quad \epsilon_v = 0.075 \quad \sigma = 10 \quad \alpha = -0.23 \quad \beta = 0.5 \quad \gamma = 0. \tag{4.8}$$

In the first figure of Fig. 5, we plot the energy curves with uniform time step sizes $\delta t = 10^{-2}$, $\delta t = 10^{-5}$ and with adaptive time steps. It is observed that the curve by adaptive time stepping coincides with the reference curve by $\delta t = 10^{-5}$, while the curve with larger time step 10^{-2} deviates from the reference curve. In the second figure, we present the evolution of adaptive time steps and observe that a wide range of time steps are used with the largest time step almost two-order of magnitude larger than the smallest time step. In the last figure, we plot evolution of the Lagrange multiplier η, and observe that η oscillates around 1 but remains to be positive.
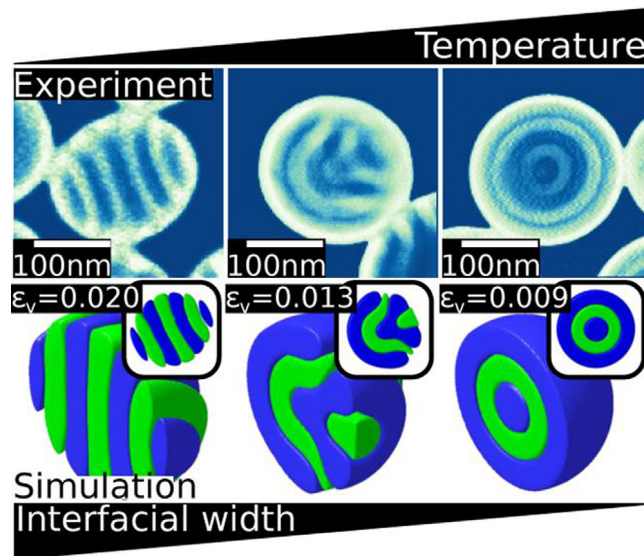
Fig. 6. Experimental results and simulations at various temperature.
Source: Taken from [28].

5. Numerical simulations of block copolymers

In this section, we consider the coupled non-local Cahn–Hilliard system (3.1)–(3.4) introduced in [22] to describe the dynamics of block copolymers. The unknowns are u and v where u describes macrophase separation into homopolymer and copolymer domains, while v describes the microphase separation within the copolymer domain; parameters M_u and M_v are mobility constants that control the speed at which order parameters u and v change; ϵ_u represents the interfacial width while ϵ_v is a parameter related to the temperature; and $\alpha, \beta, \gamma, \sigma$ are modeling parameters. The phase parameter σ represents a long range interaction that is needed to obtain particles with a fine structure, such as ellipsoids. The coupling parameter α causes symmetry-breaking between microphase separated domains and by changing its value we are able to control the interaction between the confined copolymer and the confining surface. The coupling parameter β affects the free energy depending of the sign of u. γ plays a similar role as α and is always taken to be zero in our simulations.

Three-dimensional simulations based on the coupled BCP model have produced very interesting phenomena which are also observed in experiments [22,27]. For example, Fig. 6 presented in [27] shows that the model can correctly capture the dynamical transformation of striped ellipsoids into onion like shapes as interfacial width decreases which corresponds to temperature increase. However, simple semi-implicit numerical schemes used in [22,27] for the above system lead to severe time step constraints in certain parameter regimes, so they are very expensive to run, particularly in three dimension.

We present below several two-dimensional numerical simulations for the coupled non-local Cahn–Hilliard system (3.1)–(3.4) by using the stabilized scheme (4.1)–(4.5) with adaptive time stepping. In all simulations, we take the uniformly distributed random function in $[-1, 1]^2$ as the initial condition.

5.1. Annealing of block copolymer

Annealing of block copolymers is an important process in reconfiguration of nanoparticles as in the morpholog-ical transformation of ellipsoids with striped lamellae [27]. The coupled Cahn–Hilliard equations (3.1)–(3.4) can correctly describe the process of annealing block copolymers [22,27]. This model make it possible to numerically simulate a variety of experimental conditions involving nanoparticles undergoing a heating process.

In our numerical simulations, we assume that a block copolymer particle is immersed in an external medium, which could be a homopolymer, a solvent, or water. To fix the idea, we shall consider the external medium as the homopolymer, with the order parameter $u = -1$ representing the homopolymer rich domain and $u = 1$ representing the BCP-rich domain, along with a smooth transitional layer of thickness ϵ_u. The order parameter v describes

(a) $u : t = 0.02$.　　　(b) $v : t = 0.02$.　　　(c) $u : t = 0.1$.　　　(d) $v : t = 0.1$.

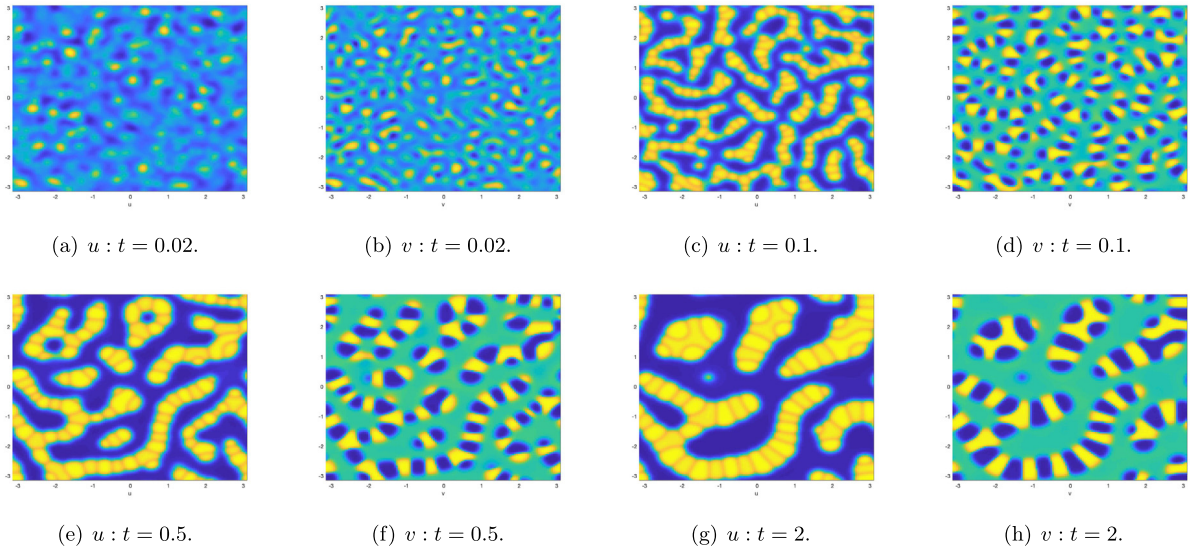(e) $u : t = 0.5$.　　　(f) $v : t = 0.5$.　　　(g) $u : t = 2$.　　　(h) $v : t = 2$.

Fig. 7. Dynamical evolution of the phase variables u, v for the Coupled-BCP model with parameters in (5.1).
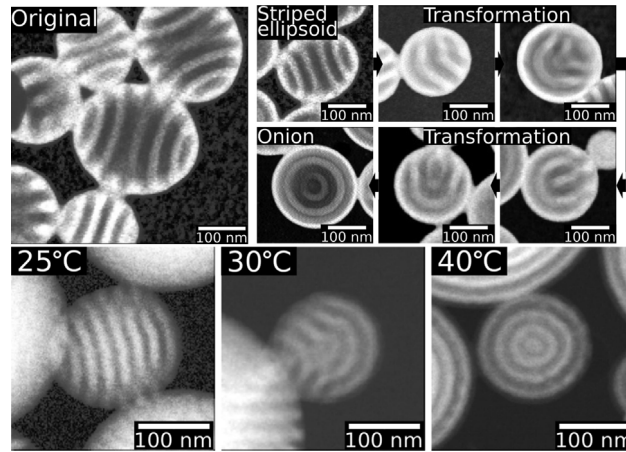

Fig. 8. Experimental results of annealing process at various temperature presented in [28].

micro separation inside the BCP domain which also acquires values from interval $[-1, 1]$ with the end points corresponding to A-type BCP and B-type BCP. The heating process starts at a given temperature T which in turn depends on the interface width ϵ_v as $T \propto \frac{1}{\epsilon_v^2}$.

In the first simulation, we set the parameters in (3.1)–(3.4) to be

$$\epsilon_u = 0.075 \quad \epsilon_v = 0.05 \quad \sigma = 10 \quad \alpha = 0.1 \quad \beta = -0.75 \quad \gamma = 0. \tag{5.1}$$

Fig. 7 shows the morphological transformations at different times. During the phase transformation, the order parameters u and v vary in a complicated manner. However at $t = 2$ which essentially reached the steady state, it is observed that v exhibits locally striped shapes, with the yellow bulk presenting A-BCP particles and blue bulk representing the B-BCP particles. The steady state morphology resembles the striped ellipsoid shape in the experimental results depicted in Fig. 8.

In the second simulation presented in Fig. 9, we used the following set of parameters

$$\epsilon_u = 0.05 \quad \epsilon_v = 0.05 \quad \sigma = 10 \quad \alpha = -0.1 \quad \beta = 0.75 \quad \gamma = 0. \tag{5.2}$$

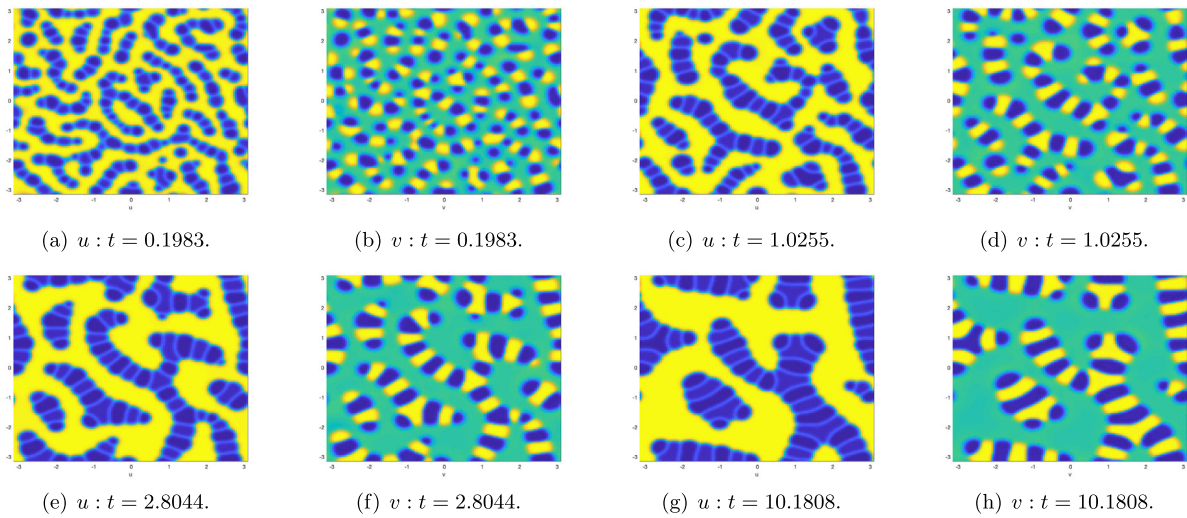Note in particular that we switched the sign of α. We observed similar configurations as in Fig. 7.

(a) $u : t = 0.1983.$ (b) $v : t = 0.1983.$ (c) $u : t = 1.0255.$ (d) $v : t = 1.0255.$

(e) $u : t = 2.8044.$ (f) $v : t = 2.8044.$ (g) $u : t = 10.1808.$ (h) $v : t = 10.1808.$

Fig. 9. Dynamical evolution of the phase variables u, v for the coupled-BCP model with parameters in (5.2).

(a) $u : t = 0.01.$ (b) $u : t = 0.05.$ (c) $u : t = 0.25.$ (d) $u : t = 20.$

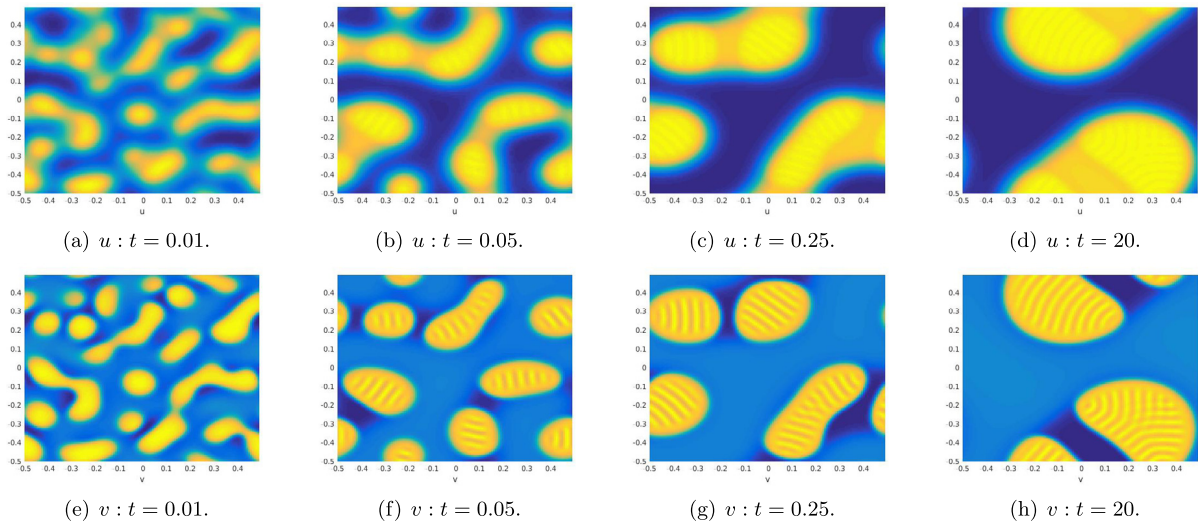(e) $v : t = 0.01.$ (f) $v : t = 0.05.$ (g) $v : t = 0.25.$ (h) $v : t = 20.$

Fig. 10. The 2D dynamical evolution of the phase variable u, v for the Coupled-BCP model with parameters in (5.3).

5.2. Annealing process at higher temperature

To offer some insight into how the interaction between copolymer segments changes with temperature. We increased the temperature T, by decreasing the interfacial width ϵ_v, in the third simulation with the parameters

$$\epsilon_u = 0.035 \quad \epsilon_v = 0.01 \quad \sigma = 10 \quad \alpha = -0.23 \quad \beta = -0.5 \quad \gamma = 0. \tag{5.3}$$

Fig. 10 shows various stages of morphology transformation at different times, where u represents the confined surface for BCP particles while v describes the dynamic process of morphological transformation for BCP particles. In the final stage, some striped ellipsoids are formed, similar to the experimental results of annealing in water depicted in Fig. 8.

To show how confined BCPs behave dynamically when the parameters are changed except ϵ_v, we set phase parameters as

$$\epsilon_u = 0.03 \quad \epsilon_v = 0.01 \quad \sigma = 10 \quad \alpha = 0.33 \quad \beta = -0.5 \quad \gamma = 0. \tag{5.4}$$
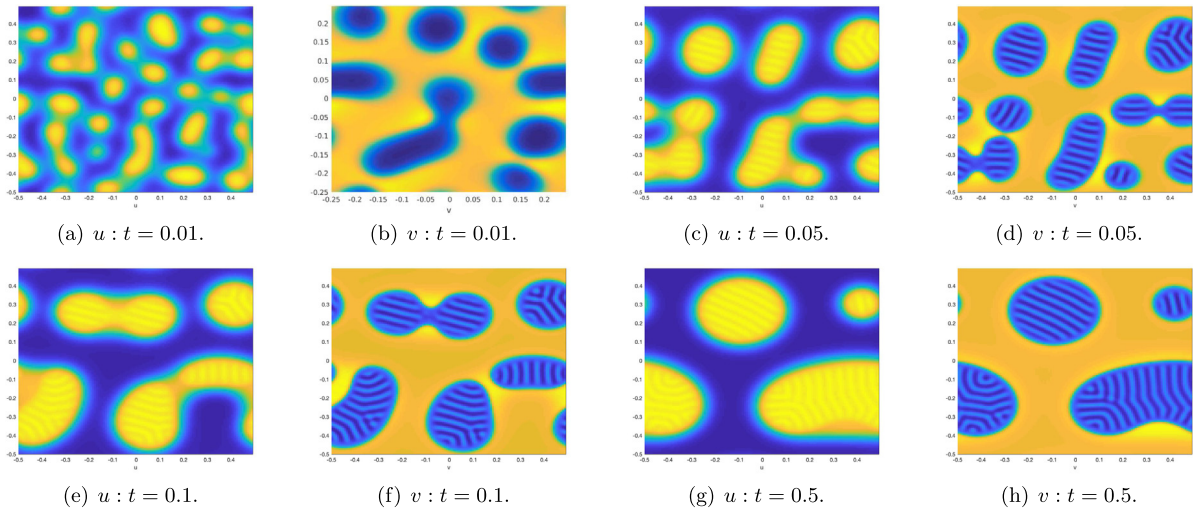
(a) $u : t = 0.01$.   (b) $v : t = 0.01$.   (c) $u : t = 0.05$.   (d) $v : t = 0.05$.

(e) $u : t = 0.1$.   (f) $v : t = 0.1$.   (g) $u : t = 0.5$.   (h) $v : t = 0.5$.

Fig. 11. The 2D dynamical evolution of the phase variable u, v for the Coupled-BCP model with parameters in (5.4).

Fig. 11 gives another type of morphology transformations at various stages. There are some striped ellipsoids and transformation shapes at time $t = 0.01, 0.05, 0.1, 0.5$ which can also observed from Fig. 8.

It is interesting to note that our two-dimensional numerical simulations captured some of the configuration shapes observed in the experiments as well as in three-dimensional simulations of [27]. Since our two-dimensional simulation can be performed with very little computational cost, compared with three-dimensional simulations using less effective schemes, it is hoped that we can use this computational tool to fine tune modeling parameters to better understand the nature of the annealing process.

6. Concluding remarks

We proposed in this paper a new Lagrange multiplier approach for general gradient flows. The new approach shares most of the nice features with the SAV approach, such as, it leads to at least second-order unconditionally energy stable schemes which can be efficiently solved with similar computational cost as the SAV approach. It also offers two additional advantages: (i) it does not require that the integral of nonlinear functional in the free energy to be bounded from below, and (ii) it dissipates the original energy. On the other hand, the new Lagrange approach requires solving a nonlinear algebraic equation with negligible additional computational cost. but it may fail to converge when the time step is large and leads to additional difficulty in its convergence and error analysis.

We presented ample numerical results to validate the stability, efficiency and accuracy of these schemes. It is found that as long as the time steps are within a reasonable range which is required for accuracy, the Newton's iteration with one as initial condition for the nonlinear algebraic equation for the Lagrange multiplier always converges in a few steps and the solution is always close to one, which is the exact solution.

The new Lagrange multiplier approach should be considered as an alternative for the SAV approach. In cases the integral of nonlinear functional in the free energy is not bounded from below or it is difficult to find a lower bound or it is desirable to have a strictly monotonic decreasing energy in the original form, the new Lagrange Multiplier approach should be used.

Although we considered only time-discretized schemes in this paper, the stability results here can be carried over to any consistent finite dimensional Galerkin type approximations since the proofs are all based on a variational formulation with all test functions in the same space as the trial functions.

We also presented two-dimensional numerical simulations for the coupled BCP model by using our new Lagrangian multiplier scheme with adaptive time stepping, and were able to capture some of the configuration shapes observed in the experiments as well as in three-dimensional simulations of [27].

We only provided stability proofs for proposed schemes in this paper. The error analysis for these schemes is nontrivial due to the nonlinear nature of this approach, and cannot be done with a similar procedure as in [29] for the original SAV approach. This will be a subject of future endeavor.

Declaration of competing interest

The authors declare that they have no known competing financial interests or personal relationships that could have appeared to influence the work reported in this paper.

Acknowledgments

References

[1] X. Tong, Christophe Beckermann, Alain Karma, Q. Li, Phase-field simulations of dendritic crystal growth in a forced flow, Phys. Rev. E 63 (6) (2001) 061601.

[2] Ryo Kobayashi, Modeling and numerical simulations of dendritic crystal growth, Physica D 63 (3–4) (1993) 410–423.

[3] R.J. Braun, B.T. Murray, Adaptive phase-field computations of dendritic crystal growth, J. Cryst. Growth 174 (1–4) (1997) 41–53.

[4] William J Boettinger, James A Warren, Christoph Beckermann, Alain Karma, Phase-field simulation of solidification, Annu. Rev. Mater. Sci. 32 (1) (2002) 163–194.

[5] SL Wang, RF Sekerka, AA Wheeler, BT Murray, SR Coriell, RJea Braun, GB McFadden, Thermodynamically-consistent phase-field models for solidification, Physica D 69 (1–2) (1993) 189–200.

[6] Alain Karma, Wouter-Jan Rappel, Phase-field method for computationally efficient modeling of solidification with arbitrary interface kinetics, Phys. Rev. E 53 (4) (1996) R3017.

[7] J.Tinsley Oden, Andrea Hawkins, Serge Prudhomme, General diffuse-interface theories and an approach to predictive tumor growth modeling, Math. Models Methods Appl. Sci. 20 (03) (2010) 477–517.

[8] Steven M Wise, John S Lowengrub, Hermann B Frieboes, Vittorio Cristini, Three-dimensional multispecies nonlinear tumor growth—I: model and numerical method, J. Theoret. Biol. 253 (3) (2008) 524–543.

[9] Alain Karma, Mathis Plapp, Spiral surface growth without desorption, Phys. Rev. Lett. 81 (20) (1998) 4444.

[10] Yu Wang, Yongmei Jin, Armen G. Khachaturyan, Phase field microelasticity modeling of dislocation dynamics near free surface and in heteroepitaxial thin films, Acta Mater. 51 (14) (2003) 4209–4223.

[11] N.B. Wilding, F. Schmid, P. Nielaba, Liquid-vapor phase behavior of a symmetrical binary fluid mixture, Phys. Rev. E 58 (2) (1998) 2201.

[12] Rodica Borcia, Michael Bestehorn, Phase-field simulations for evaporation with convection in liquid-vapor systems, Eur. Phys. J. B 44 (1) (2005) 101–108.

[13] Michael J Borden, Clemens V Verhoosel, Michael A Scott, Thomas JR Hughes, Chad M Landis, A phase-field description of dynamic brittle fracture, Comput. Methods Appl. Mech. Engrg. 217 (2012) 77–95.

[14] Christian Miehe, Fabian Welschinger, Martina Hofacker, Thermodynamically consistent phase-field models of fracture: variational principles and multi-field FE implementations, Internat. J. Numer. Methods Engrg. 83 (10) (2010) 1273–1311.

[15] Qiang Du, Xiaobing Feng, The phase field method for geometric moving interfaces and their numerical approximations, 2019, arXiv preprint arXiv:1902.04924.

[16] Jie Shen, Jie Xu, Jiang Yang, The scalar auxiliary variable (SAV) approach for gradient flows, J. Comput. Phys. 353 (2018) 407–416.

[17] Jie Shen, Jie Xu, Jiang Yang, A new class of efficient and robust energy stable schemes for gradient flows, SIAM Rev. 61 (3) (2019) 474–506.

[18] Qing Cheng, Jie Shen, Multiple scalar auxiliary variable (MSAV) approach and its application to the phase-field vesicle membrane model, SIAM J. Sci. Comput. 40 (6) (2018) A3982–A4006.

[19] Xiaofeng Yang, Lili Ju, Efficient linear schemes with unconditional energy stability for the phase field elastic bending energy model, Comput. Methods Appl. Mech. Engrg. 315 (2017) 691–712.

[20] Francisco Guillén-González, Giordano Tierra, On linear schemes for a Cahn–Hilliard diffuse interface model, J. Comput. Phys. 234 (2013) 140–171.

[21] Santiago Badia, Francisco Guillén-González, Juan Vicente Gutiérrez-Santacreu, Finite element approximation of nematic liquid crystal flows using a saddle-point structure, J. Comput. Phys. 230 (4) (2011) 1686–1706.

[22] Edgar Avalos, Takeshi Higuchi, Takashi Teramoto, Hiroshi Yabu, Yasumasa Nishiura, Frustrated phases under three-dimensional confinement simulated by a set of coupled Cahn–Hilliard equations, Soft Matter 12 (27) (2016) 5905–5914.

[23] J. Villain, Continuum models of crystal growth from atomic beams with and without desorption, J. Phys. I 1 (1) (1991) 19–42.

[24] Qing Cheng, Jie Shen, Xiaofeng Yang, Highly efficient and accurate numerical schemes for the epitaxial thin film growth models by using the SAV approach, J. Sci. Comput. 78 (3) (2019) 1467–1487.

[25] Hector Gomez, Thomas J.R. Hughes, Provably unconditionally stable, second-order time-accurate, mixed variational methods for phase-field models, J. Comput. Phys. 230 (13) (2011) 5310–5327.

[26] Jie Shen, Tao Tang, Jiang Yang, On the maximum principle preserving schemes for the generalized Allen–Cahn equation, Commun. Math. Sci. 14 (2016) 1517–1534.

[27] Divya Varadharajan, Hatice Turgut, Joerg Lahann, Hiroshi Yabu, Guillaume Delaittre, Surface-reactive patchy nanoparticles and nanodiscs prepared by tandem nanoprecipitation and internal phase separation, Adv. Funct. Mater. 28 (39) (2018) 1800846.

[28] Edgar Avalos, Takashi Teramoto, Hideaki Komiyama, Hiroshi Yabu, Yasumasa Nishiura, Transformation of block copolymer nanoparticles from ellipsoids with striped lamellae into onionlike spheres and dynamical control via coupled Cahn–Hilliard equations, ACS Omega 3 (1) (2018) 1304–1314.

[29] Jie Shen, Jie Xu, Convergence and error analysis for the scalar auxiliary variable (SAV) schemes to gradient flows, SIAM J. Numer. Anal. 56 (5) (2018) 2895–2912.